Ultrasonics Sonochemistry 21 (2014) 53–59

Contents lists available at SciVerse ScienceDirect

Ultrasonics Sonochemistry

journal homepage: www.elsevier.com/locate/ultson

Theoretical estimation of the temperature and pressure within collapsing acoustical bubbles

Slimane Merouani [a], Oualid Hamdaoui [a,*], Yacine Rezgui [b], Miloud Guemini [b]

[a] Laboratory of Environmental Engineering, Department of Process Engineering, Faculty of Engineering, Badji Mokhtar – Annaba University, P.O. Box 12, 23000 Annaba, Algeria
[b] Laboratory of Applied Chemistry and Materials Technology, University of Oum El-Bouaghi, P.O. Box 358, 04000 Oum El Bouaghi, Algeria

ARTICLE INFO

Article history:
Received 20 April 2013
Received in revised form 13 May 2013
Accepted 20 May 2013
Available online 29 May 2013

Keywords:
Cavitation bubbles
Sonochemical reaction
Computer simulations
·OH radical
Bubble temperature

ABSTRACT

Formation of highly reactive species such as ·OH, H·, HO_2· and H_2O_2 due to transient collapse of cavitation bubbles is the primary mechanism of sonochemical reaction. The crucial parameters influencing the formation of radicals are the temperature and pressure achieved in the bubble during the strong collapse. Experimental determinations estimated a temperature of about 5000 K and pressure of several hundreds of MPa within the collapsing bubble. In this theoretical investigation, computer simulations of chemical reactions occurring in an O_2-bubble oscillating in water irradiated by an ultrasonic wave have been performed for diverse combinations of various parameters such as ultrasound frequency (20–1000 kHz), acoustic amplitude (up to 0.3 MPa), static pressure (0.03–0.3 MPa) and liquid temperature (283–333 K). The aim of this series of computations is to correlate the production of ·OH radicals to the temperature and pressure achieved in the bubble during the strong collapse. The employed model combines the dynamic of bubble collapse in acoustical field with the chemical kinetics of single bubble. The results of the numerical simulations revealed that the main oxidant created in an O_2 bubble is ·OH radical. The computer simulations clearly showed the existence of an optimum bubble temperature of about 5200 ± 200 K and pressure of about 250 ± 20 MPa. The predicted value of the bubble temperature for the production of ·OH radicals is in excellent agreement with that furnished by the experiments. The existence of an optimum bubble temperature and pressure in collapsing bubbles results from the competitions between the reactions of production and those of consumption of ·OH radicals at high temperatures.

1. Introduction

Acoustic cavitation is the phenomenon observed when ultrasound of sufficient intensity is transmitted through a liquid causing micron-sized gas and vapor bubbles to oscillate, grow and violently implode giving rise to extreme, but localized, conditions within the collapsed cavities (extremely high temperatures and pressures) [1]. Such conditions are primarily responsible for the chemical effects (sonochemistry) associated with acoustic cavitation in liquids [2]. The extremely high temperatures and pressures formed in collapsing cavitation bubbles in aqueous solutions lead to the thermal dissociation of the trapped water vapor into H· and ·OH radicals, and with other species present, various other reactive species such as HO_2·, O and H_2O_2 may form [2,3]. A parallel reaction pathways exist where volatile solutes may evaporate into the bubble and be pyrolysed by the high core temperatures [2,4]. The radical species produced can recombine, react with other gaseous species present in the cavity, or diffuse out of the bubble into the bulk liquid medium to serve as oxidants [5]. Among all the oxidants created in the bubble, ·OH radical is of primary interest because of its high potential of oxidation. Under certain conditions bubble collapse can also result in light emission, sonoluminescence, originating from the hot core of the bubble during the final stages of collapse [4,6].

Experimental determinations of the temperature within a cavitation bubble have been made by a number of research groups. By fitting the experimentally recorded single bubble sonoluminescence spectra, temperatures in the range of 5000–20,000 K have been estimated [7]. However, experimental estimation of the temperature within the collapsing bubbles based on multibubble sonochemistry and sonoluminescence are reported to be between 750 and 6000 K. Misík et al. [8], using the kinetic isotope effect in an EPR spin-trapping study of the sonolyse of H_2O/D_2O mixtures, found that the cavitation temperature determined was dependent on the specific spin trap used and fall in the range of 1000–4600 K. Misík and Reisz [9] used the kinetic isotope effect in the ultrasound induced production of radicals in organic liquids to estimate the temperature during cavitation. The bubble temperature was found to be in the range 750–6000 K. Suslick et al. [10], using comparative rate thermometry in alkane solutions, postulated that there

* Corresponding author. Tel./fax: +213 (0)38876560.
E-mail addresses: ohamdaoui@yahoo.fr, oualid.hamdaoui@univ-annaba.org (O. Hamdaoui).

1350-4177/$ - see front matter © 2013 Elsevier B.V. All rights reserved.
http://dx.doi.org/10.1016/j.ultsonch.2013.05.008

Nomenclature

A_f (A_r)	pre-exponential factor of the forward (reverse) reaction [($cm^3\ mol^{-1}\ s^{-1}$) for two body reaction and ($cm^6\ mol^{-2}\ s^{-1}$) for three body reaction]
b_f (b_r)	temperature exponent of the forward (reverse) reaction
c	speed of sound in the liquid medium ($m\ s^{-1}$)
E_{af} (E_{ar})	activation energy of the forward (reverse) reaction ($cal\ mol^{-1}$)
f	frequency of ultrasonic wave (Hz)
I_a	acoustic intensity of ultrasonic irradiation ($W\ m^{-2}$)
k_f (k_r)	forward (reverse) reaction constant [($cm^3\ mol^{-1}\ s^{-1}$) for two body reaction and ($cm^6\ mol^{-2}\ s^{-1}$) for three body reaction]
p	pressure inside a bubble (Pa)
p_∞	ambient static pressure (Pa)
P_A	amplitude of the acoustic pressure (Pa)
P_v	vapor pressure of water (Pa)
P_{g0}	initial gas pressure (Pa)
R	radius of the bubble (m)
R_{max}	maximum radius of the bubble (m)
R_0	ambient bubble radius (m)
t	time (s)
T	temperature inside a bubble (K)
T_c	critical temperature of water (374.2 °C)
T_∞	ambient liquid temperature (K)

Greek letters

γ	specific heat ratio (c_p/c_v) of the gas mixture
σ	surface tension of liquid water ($N\ m^{-1}$)
ρ	density of liquid water ($Kg\ m^{-3}$)
μ	viscosity of liquid water ($N\ m^{-2}\ s$)

are two regions of sonochemical reactivity: a gas phase zone within the collapsing cavity with an estimated temperature and pressure of 5200 ± 650 K and 50 MPa, respectively, and a thin liquid layer immediately surrounding the collapsing cavity with an estimated temperature of ~1900 K. Henglein and coworkers [11], by means of sonolysis of methane in argon saturated water, estimated the bubble core temperature to be in the range of 1930–2720 K, depending upon the concentration of methane and argon present in water (the temperature decreased with an increase in the percentage of methane). Using *tert*-butanol sonolysis as means, Tauber et al. [12] estimated the bubble temperature to be in the range 2300–3600 K. The higher temperature was obtained for fresh water, whereas the lower temperature was obtained for solution with the highest concentration of *tert*-butanol. Recently, Ashokkumar and coworkers measured the bubble temperature at different conditions using the Methyl Radical Recombination (MRR) method [13–15]. They found that the maximum bubble temperature is obtained in fresh water and is greatly influenced by the frequency of ultrasound. They estimated maximum temperatures of about 3400 ± 200 K at 20 kHz, 4300 ± 200 K at 366 kHz and 3700 ± 200 K (6200 K [15]) at 1056 kHz [13,14].

In the present study, we have theoretically estimated the optimum temperature of collapsing bubble for the production of the oxidants, i.e. ·OH radicals. The used model combines the dynamic of bubble collapse in acoustical field propagated in water with a chemical kinetics consisting in nineteen reversible chemical reactions occurring at high temperatures during the strong collapse of the bubble. A series of computations were performed for more than 400 combinations between various parameters including ultrasound frequency in the range 20–1000 kHz, acoustic amplitude up to 0.3 MPa, static pressure from 0.03 to 0.3 MPa and liquid temperature between 283 and 333 K.

2. Model

2.1. Bubble dynamics model

The physical situation of the model is that of a gas and vapor filled spherical bubble isolated in water oscillating under the action of a sinusoidal sound wave. The temperature and pressure in the bubble are assumed to be spatially uniform and the gas content of the bubble behaves as an ideal gas [16]. The radial dynamics of the bubble is described by the Keller–Miksis equation [17,18]:

$$\left(1-\frac{\dot{R}}{c}\right)R\ddot{R}+\frac{3}{2}\left(1-\frac{\dot{R}}{3c}\right)\dot{R}^2=\frac{1}{\rho_L}\left(1+\frac{\dot{R}}{c}+\frac{R}{c}\frac{d}{dt}\right)\times\left[p-p_\infty-\frac{2\alpha}{R}-4\mu\frac{\dot{R}}{R}+P_A\sin(2\pi ft)\right] \quad (1)$$

in this equation dots denote time derivatives (d/dt), R is the radius of the bubble, c is the speed of sound in the liquid, ρ_L is the density of the liquid, σ is the surface tension, μ is the liquid viscosity, p is the pressure inside the bubble, p_∞ is the ambient static pressure, P_A is the acoustic amplitude and f is the sound frequency. The acoustic amplitude P_A is correlated with the acoustic intensity I_a, or power per unit area, as $P_A = (2I_a\rho_L c)^{1/2}$ [19]. Eq. (1) is only accurate to first order in the bubble wall Mach number ($\dot{R}/c$) but, for all acoustic amplitudes in this study, this level of accuracy is sufficient (the speed of the bubble wall ($|\dot{R}|$) at the collapse never exceeds the sound velocity in the liquid c, which is the assumption used in the derivation of the equation [17]).

In the present model, the expansion of the bubble is considered as isothermal and its total compression (implosion phase) is treated as adiabatic [20]. This assumption is very accepted as for high frequencies the lifetime of the bubble is very short and the collapse event occurs rapidly. We assume also that the vapor pressure in the bubble remains constant during the bubble expansion phase and there is no gas diffusion during expansion and no mass and heat transfer of any kind during collapse. There exist in the literature some research studies that include these effects [20–22]. For a comparative point of view, the inclusion of these effects, leading to a realistic situation, might change the absolute values of the predicted collapse temperature and pressure but definitively will not change the predicted trends including the qualitative variation of the maximum radius, the collapse time and the maximum collapse temperature with variation in operational conditions. Additionally, the importance of mass and heat transfer occur over multiple cycles of oscillation changing, in this case, the internal composition of the vapor phase. Consequently, as the present numerical calculations were carried out for one acoustic period, the mass and heat transfer will not also affect significantly the quantitative bubble yield, predicted in one acoustic period. So, in order to reduce computational parameters, the current model takes, as input, initial bubble vapor content and neglects mass and heat transfer during bubble expansion and collapse.

On the basis of the above assumptions, the pressure and temperature inside the bubble at any instant during adiabatic phase can be calculated from the bubble size, using the adiabatic law:

$$p = \left[P_v + P_{g0}\left(\frac{R_0}{R_{\max}}\right)^3\right]\left(\frac{R_{\max}}{R}\right)^{3\gamma} \quad (2)$$

$$T = T_\infty\left(\frac{R_{\max}}{R}\right)^{3(\gamma-1)} \quad (3)$$

where P_v is the vapor pressure, $P_{g0} = p_\infty + (2\sigma/R_0) - P_v$ is the gas pressure in the bubble at its ambient state ($R = R_0$), R_0 is the ambient bubble radius, T_∞ is the bulk liquid temperature, R_{max} is the maximum radius of the bubble and γ is the ratio of specific heats capacities (c_p/c_v) of the gas/vapor mixture. It is important to notice here that the assumption of spatial uniform pressure and temperature inside the bubble is valid as long as inertia effects are negligible and the velocity of the bubble wall is below the speed of sound in the vapor/gas mixture. This assumption was justified in detail in the paper published by Kamath et al. [23]. Also, Yasui et al. [22] and Fujikawa et Akamatzu [24] pointed out in their models which include heat transfer that the bubble temperature and pressure are roughly uniform except at a very thin layer, called thermal boundary, near the bubble wall.

2.2. Estimation of physical properties

Several physical properties (saturated vapor pressure, density, surface tension, viscosity and sound velocity) in the above equations change with the liquid temperature T_∞ (water is the liquid medium in this study) and the static pressure p_∞. The equations for the physical properties have been described in our previous work [25].

2.3. Chemical kinetics model

For a bubble initially containing oxygen and water vapor, a kinetic mechanism consisting in nineteen reversible elementary chemical reactions (Table 1) is taken into account involving O_2, H_2O, ·OH, H·, O, HO_2·, H_2 and H_2O_2 chemical species. The scheme in Table 1 has been partially validated from hydrogen flame studies [26] as well as shock-tube and reactor-type experiments [27]. It has also been used by many research groups in sonochemistry and sonoluminescence [20,23].

Rate expressions for the chemical reactions consider elementary reversible reactions involving k chemical species, which can be represented in the general form as

$$\sum_{k=1}^{K}\upsilon'_{ki}X_k \leftrightarrow \sum_{k=1}^{K}\upsilon''_{ki}X_k \quad (4)$$

in which υ_{ki} in the stoichiometric coefficients of the ith reaction and X_k is the chemical symbol for the kth species. The superscript $'$ indicates forward stoichiometric coefficients, while $''$ indicates reverse stoichiometric coefficients. The production rate of the kth species can be written as a summation of the rate of the variables for all reactions involving the kth species:

$$\dot{w}_k = \sum_{i=1}^{I}(\upsilon''_{ki} - \upsilon'_{ki})r_i \quad (k = 1, \ldots, K) \quad (5)$$

The rate r_i for the ith reaction is given by the difference of the forward and reverse rates as

$$r_i = k_{f_i}\prod_{k=1}^{K}[X_k]^{\upsilon'_{ki}} - k_{r_i}\prod_{k=1}^{K}[X_k]^{\upsilon''_{ki}} \quad (6)$$

where $[X_k]$ is the molar concentration of the kth species and k_{fi} and k_{ri} are the forward and reverse rate constants of the ith reaction, respectively. The forward and reverse rate constants for the ith reactions are assumed to have the following Arrhenius temperature dependence:

$$K_{f_i} = A_{fi}T^{b_{fi}}\exp\left(-\frac{E_{a_{f_i}}}{R_gT}\right) \quad (7)$$

$$K_{ri} = A_{ri}T^{b_{ri}}\exp\left(-\frac{E_{a_{ri}}}{R_gT}\right) \quad (8)$$

where R_g is the universal gas constant, A_{fi} (A_{ri}) is the pre-exponential factor, b_{fi} (b_{ri}) is the temperature exponent and E_{fi} (E_{ri}) is the activation energy. Arrhenius parameters of each chemical reaction in Table 1 are obtained from the NIST Chemical Kinetics Database [28].

2.4. Procedure of the numerical simulation

The simulation of the reactions system (Table 1) occurring in the bubble starts at the beginning of the adiabatic phase (time corresponding to R_{max}). The input parameters of the reactions system are the composition of the bubble on water vapor and oxygen at

Table 1
Scheme of the possible chemical reactions inside an O_2 cavitation bubble. M is the third body. Subscript "*f*" denotes the forward reaction and "*r*" denotes the reverse reaction. *A* is in ($cm^3\ mol^{-1}\ s^{-1}$) for two body reaction [($cm^6\ mol^{-2}\ s^{-1}$) for a three body reaction], and E_a is in ($cal\ mol^{-1}$).

Reaction	A_f	b_f	E_{af}	A_r	b_r	E_{ar}
$H_2O + M \leftrightarrow H\cdot + \cdot OH + M$	1.912×10^{23}	−1.83	1.185×10^5	2.200×10^{22}	−2.00	0.00
$O_2 + M \leftrightarrow O + O + M$	4.515×10^{17}	−0.64	1.189×10^5	6.165×10^{15}	−0.50	0.00
$\cdot OH + M \leftrightarrow O + H\cdot + M$	9.88×10^{17}	−0.74	1.021×10^5	4.714×10^{18}	−1.00	0.00
$H\cdot + O_2 \leftrightarrow O + \cdot OH$	1.915×10^{14}	0.00	1.644×10^4	5.481×10^{11}	0.39	-2.93×10^2
$H\cdot + O_2{+}M \leftrightarrow HO_2\cdot + M$	1.475×10^{12}	0.60	0.00	3.090×10^{12}	0.53	4.887×10^4
$O + H_2O \leftrightarrow \cdot OH + \cdot OH$	2.970×10^6	2.02	1.340×10^4	1.465×10^5	2.11	-2.904×10^3
$HO_2 + H\cdot \leftrightarrow H_2 + O_2$	1.660×10^{13}	0.00	8.230×10^2	3.164×10^{12}	0.35	5.551×10^4
$HO_2\cdot + H\cdot \leftrightarrow \cdot OH + \cdot OH$	7.079×10^{13}	0.00	2.950×10^2	2.027×10^{10}	0.72	3.684×10^4
$HO_2\cdot + O \leftrightarrow \cdot OH + O_2$	3.250×10^{13}	0.00	0.00	3.252×10^{12}	0.33	5.328×10^4
$HO_2\cdot + \cdot OH \leftrightarrow H_2O + O_2$	2.890×10^{13}	0.00	-4.970×10^2	5.861×10^{13}	0.24	6.908×10^4
$H_2 + M \leftrightarrow H\cdot + H\cdot + M$	4.577×10^{19}	−1.40	1.044×10^5	1.146×10^{20}	−1.68	8.200×10^2
$O + H_2 \leftrightarrow H\cdot + \cdot OH$	3.820×10^{12}	0.00	7.948×10^3	2.667×10^4	2.65	4.880×10^3
$\cdot OH + H_2 \leftrightarrow H\cdot + H_2O$	2.160×10^8	1.52	3.450×10^3	2.298×10^9	1.40	1.832×10^4
$H_2O_2 + O_2 \leftrightarrow HO_2\cdot + HO_2\cdot$	4.634×10^{16}	−0.35	5.067×10^4	4.200×10^{14}	0.00	1.198×10^4
$H_2O_2 + M \leftrightarrow \cdot OH + \cdot OH + M$	2.951×10^{14}	0.00	4.843×10^4	1.00×10^{14}	−0.37	0.00
$H_2O_2 + H\cdot \leftrightarrow H_2O + \cdot OH$	2.410×10^{13}	0.00	3.970×10^3	1.269×10^8	1.31	7.141×10^4
$H_2O_2 + H\cdot \leftrightarrow H_2 + HO_2\cdot$	6.025×10^{13}	0.00	7.950×10^3	1.041×10^{11}	0.70	2.395×10^4
$H_2O_2 + O \leftrightarrow \cdot OH + HO_2\cdot$	9.550×10^6	2.00	3.970×10^3	8.660×10^3	2.68	1.856×10^4
$H_2O_2 + \cdot OH \leftrightarrow H_2O + HO_2\cdot$	1.000×10^{12}	0.00	0.00	1.838×10^{10}	0.59	3.089×10^4

Table 2
The ranges of parameters used in the present computation study. All numerical simulations were performed for bubbles initially composed of oxygen and water vapor.

Frequency f (kHz)	Acoustic amplitude P_A (MPa)	Static pressure p_∞ (MPa)	Liquid temperature T_∞ (K)	Range of initial radius R_0 (μm)	Number of combinations
20	0.1	0.08, 0.1	298	1–25[a,b]	40
200	0.15–0.3	0.1	293	0.25–18[c,d]	70
300	0.15–0.3	0.1 (0.03–0.3 MPa for T_∞ = 293 K)	293 (283–333 K for p_∞ = 0.1 MPa)	0.25–12[d,e,f]	140
500	0.15–0.3	0.1	293–323	0.25–7[d]	100
1000	0.15–0.3	0.1	293	0.25–3.5[d,e,g]	60

[a] Burdin et al. [31].
[b] Tsochatzidis et al. [32].
[c] Thiemann et al. [33].
[d] Merouani et al. [35].
[e] Labouret and Frohly [34].
[f] Yasui et al. [36].
[g] Yasui et al. [37].

this point, the temperature and pressure profiles in the bubble during adiabatic phase and the collapse time. All these parameters were obtained by solving the dynamics equation (Eq. (1)). As the bubble temperature increases during the adiabatic phase, the reaction system evolves and radicals start to form by thermal dissociation of H_2O and O_2 molecules in the bubble (Reactions (1) and (2) in Table 1). Thus, the composition of the bubble for all species expected to be present (O_2, H_2O, ·OH, H·, O, HO_2·, H_2 and H_2O_2) was determined at any temperature during the collapse phase. The simulation of the reactions system was stopped after the end of the bubble collapse. It should be also noticed that the effect of the chemical reaction (heat of reaction) occurring in the cavity on the bubble dynamics is known to be not significant [21,29]. The dynamics output results, thus, will not greatly affected by the chemical reactions. This effect is not taken into account in the present numerical investigation.

3. Results and discussion

The present numerical simulations have been performed for ultrasound frequencies in the range of 20–1000 kHz because it is the range of frequencies commonly used in sonochemistry. Another important factor for the numerical calculations is the ambient bubble radius R_0 of bubbles that can produce sonochemical effects. Experimental [30–34] and theoretical [35–37] studies demonstrated that the ambient size of the cavitation bubbles has an interval rather than a fixed size. Moreover, the range itself of the ambient radius is strongly dependent on the experimentally controllable parameters, particularly on the ultrasound frequency. In this study, the ranges of ambient radius R_0 for the numerical simulations are selected as function of frequency according to the experimental and theoretical results. Detailed informations about the ranges of parameters used in the present numerical study are illustrated in Table 2.

3.1. Bubble dynamics and production of the oxidants

In Fig. 1, the calculated bubble radius is shown as function of time for one acoustic cycle with the liquid pressure for an ultrasonic frequency of 500 kHz and pressure amplitude of 0.25 MPa when the ambient radius of an isolated oxygen bubble is 3 μm. It is seen that a bubble initially expands during the rarefaction phase of an ultrasonic wave and when the liquid pressure becomes greater than 1 atm, at the compression phase, the bubble expansion slows down. Finally, the bubble begins to collapses violently and then expands again. The maximum bubble radius is 10.22 μm and the timescale of the bubble expansion is about 3 times larger than that of the collapse.

In Fig. 2, the calculated bubble radius and the temperature inside a bubble are shown as function of time during the collapse phase. The bubble collapses very violently and the temperature and pressure inside a bubble increase suddenly at the end of the bubble collapse up to 4600 K and 1400 atm (~140 MPa) and then decrease very soon.

In Fig. 3, the mole fraction of each chemical species in the bubble is shown as function of time at around the end of the bubble collapse. The temperature profile inside the bubble is also included in this figure. In O_2-satured water, the main bubble contents are oxygen and water vapor. At the final stage of the bubble collapse when the temperature and pressure inside a bubble increased drastically, more than 20% of oxygen and 40% of water vapor are dissociated in the bubble and many chemical products such as H_2, HO_2·, H·, O and ·OH are created in the bubble. It is seen that the amount of each chemical oxidants attained their upper limit at the end of the bubble collapse (Fig. 3). From Fig. 3, it is also evident that ·OH radicals is the dominant radical species produced in the bubble and constitute alone more than 60% of the oxidants (·OH, H·, O, HO_2· and H_2O_2) created in the bubble. In the following Section 3.2 we will, thus, employed only the mole fraction of ·OH radicals formed in the bubble per collapse as means to represent the activity of the collapsing bubble.

The chemical analysis performed for the case of Fig. 3 showed that ·OH radicals are formed in the bubble mainly by the following reactions: $H_2O + M \rightarrow H^\cdot + {}^\cdot OH + M$, $H_2O_2 + M \rightarrow 2{}^\cdot OH$ and $HO_2^\cdot + O \rightarrow {}^\cdot OH + O_2$ and consumed mainly thought $2{}^\cdot OH \rightarrow O + H_2O$, $HO_2^\cdot + {}^\cdot OH \rightarrow H_2O + O_2$ and ·OH + M → H· + O + M. Oxygen atoms are formed mainly thought $2{}^\cdot OH \rightarrow O + H_2O$ and ·OH + M → H· + O + M and consumed mainly thought $O + {}^\cdot OH \rightarrow O_2 + H^\cdot$, $HO_2^\cdot + O \rightarrow {}^\cdot OH + O_2$ and 2O + M → O_2 + M. Perhydroxyl radicals are formed mainly thought $H^\cdot + O_2 + M \rightarrow HO_2^\cdot + M$ and consumed mainly thought $HO_2^\cdot + {}^\cdot OH \rightarrow H_2O + O_2$, $O + HO_2^\cdot \rightarrow {}^\cdot OH + O_2$, $2HO_2^\cdot \rightarrow H_2O_2 + O_2$ and $2HO_2^\cdot + H^\cdot \rightarrow H_2O_2 + {}^\cdot OH$. Hydrogen atoms are formed by $H_2O + M \rightarrow H^\cdot + {}^\cdot OH + M$, $O + {}^\cdot OH \rightarrow O_2 + H^\cdot$ and ·OH + M → O + H· + M and consumed mainly thought a reaction $H^\cdot + O_2 + M \rightarrow HO_2^\cdot + M$. Molecular hydrogen was not found to be formed by recombination of hydrogen atoms (H· + H· + M → H_2 + M) as reported in the literature but thought a reaction $H^\cdot + {}^\cdot OH \rightarrow O + H_2$ and consumed mainly by $^\cdot OH + H_2 \rightarrow H^\cdot + H_2O$. Also, Hydrogen peroxide has not seen to be formed in the bubble at appreciable amount because at higher temperatures H_2O_2 is unstable and dissociates inside a bubble mainly thought a reaction $H_2O_2 + M \rightarrow 2{}^\cdot OH + M$.

3.2. Optimum bubble temperature and pressure

The mole fraction of ·OH radical created in the bubble per collapse for each case of the diverse combinations (more than 400

points of combination (Table 2)) was related to the corresponding maximum temperature and pressure achieved in the bubble at the collapse. The correlation between the bubble temperature and the mole fraction of ·OH radicals created per collapse is shown in Fig. 4. The correlation between the pressure inside a bubble at the collapse and the mole fraction of ·OH radicals formed in the bubble per collapse is shown in Fig. 5. As can be seen, two valleys of points were obtained constituting the mole fraction of ·OH radicals created per collapse as function of temperature (Fig. 4) and pressure (Fig. 5). The numerical simulations clearly showed the existence of an optimum bubble temperature of about 5200 ± 200 K and pressure of about 250 ± 20 MPa for the production of ·OH radicals, as can be seen in Figs. 4 and 5. Suslick and coworkers estimated, by kinetic measurements, a maximum bubble temperature of 5200 ± 650 K [10]. They also determined a temperature of 5100 ± 200 K, using a spectroscopic measurements during multi-bubble sonoluminescence (MBSL) emitted from excited states of free metal atoms [38,39]. Ashokkumar and coworkers [15] determined a maximum bubble temperature between 5000 K and 6000 K using the Methyl Radical Recombination Method (MMR). Thus, the optimum bubble temperature predicted in our study (5200 ± 200 K) is in excellent agreement with the experimentally estimated bubble temperatures. Additionally, Suslick and coworkers [40] experimentally determined an average pressure of about 150 MPa inside a single-sonoluminescing bubble. Upon stronger acoustic driving of the bubble, they estimated a maximum pressure of about 370 MPa [40]. Thus, the optimum value of pressure, 250 ± 20 MPa, predicted in our theoretical study for oxygen bubbles is in the same order of magnitude with the experimentally estimated pressures. The observed difference may be due to the different saturating gases: O_2 for our theoretical study and Ar for Suslick's studies.

Another important statement that can be made from Fig. 4 is that although all bubbles having temperatures at the collapse in the range of 1000–7000 K are actives, the more active bubbles are those achieving temperatures between 4000 and 6000 K, which is nearly the same range of experimentally bubble temperatures reported in the literature [10–15]. Correspondingly, all bubbles achieving pressures at the collapse between 10 MPa and 400 MPa are active and can produce chemical effect (Fig. 5). This predicted

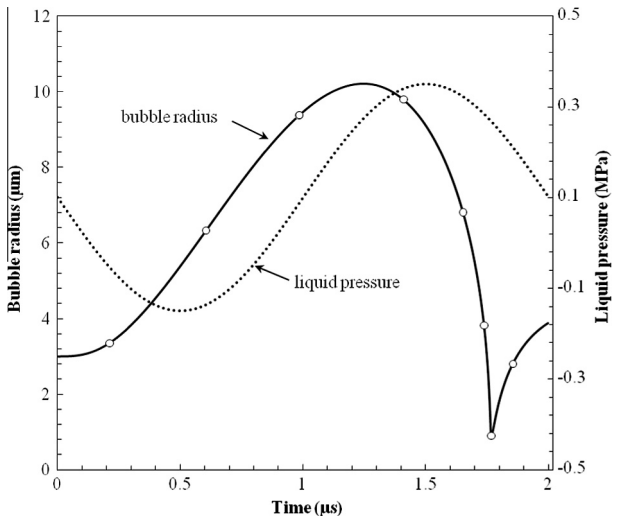

Fig. 1. Bubble radius and liquid pressure as a function of time for one acoustic cycle (2 μs). The liquid pressure is the sum of the acoustic pressure $-P_A \sin 2\pi ft$ and the static pressure P_∞ (conditions: ambient bubble radius: 3 μm; frequency: 500 kHz; acoustic amplitude: 0.25 MPa; temperature: 293 K; static pressure: 0.1 MPa). The maximum radius is 10.22 μm, the lifetime of the bubble is about 1.765 μs and the collapse time is about 0.52 μs.

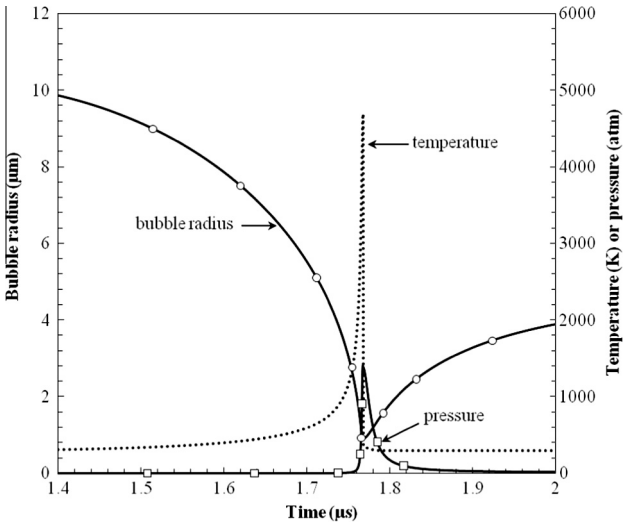

Fig. 2. Bubble radius and temperature and pressure inside a bubble as function of time during the collapse phase of the bubble, for the same conditions as in Fig. 1. The horizontal axis is only for 0.6 μs. A maximum bubble temperature of about 4600 K and pressure of about 1400 atm (~140 MPa) are achieved at the end of the collapse. In this figure, we preferred to present the pressure inside a bubble in atm rather than MPa to only present it on the same axis (secondary axis) with the bubble temperature.

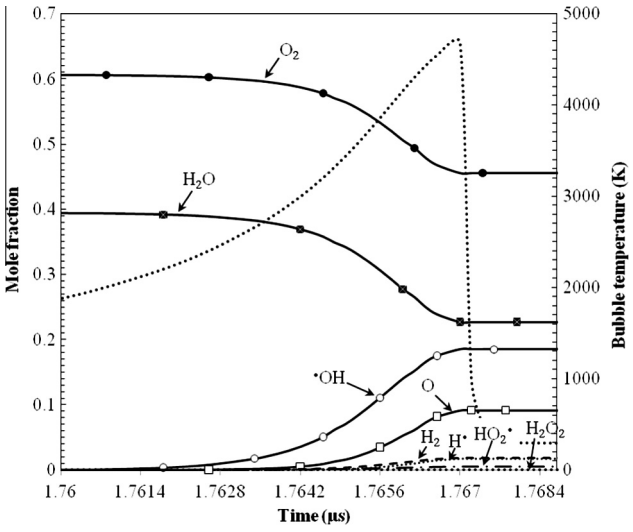

Fig. 3. Mole fraction of each chemical species inside a bubble as function of time at around the end of the bubble collapse. Results obtained for the same conditions as in Fig. 1. The horizontal axis is only for 0.0084 μs. It is clear that ·OH radical is the main product formed inside a bubble at the end of the bubble collapse.

range of pressures, 10–400 MPa, cover the range of pressures determined experimentally, which is from 30 to 400 MPa [39].

It is possible that the distribution of the cavitation bubble temperature and pressure at the collapse with respect to the ambient bubble radius is the reason for the trends observed in Figs. 4 and 5. To verify this point, the distribution of the cavitation properties (temperature and pressure) are plotted in Fig. 6 as function of ambient bubble radius for some conditions of Table 2. From Fig. 6, it is observed that the distribution curves are not homogeneous for each range (linear for 20 kHz, decreases sharply for 200 and 300 and presents a maximum of about 7500 K (Fig. 6a) and 900 MPa (Fig. 6b) for smallest bubble radii at 500 and 1000 kHz)

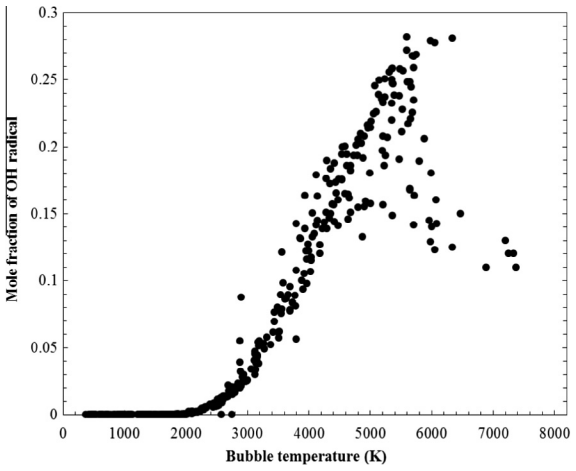

Fig. 4. The correlation between bubble temperature at the collapse and the mole fraction of ·OH radical formed inside a bubble per collapse for oxygen/water vapor bubbles. The numerical results were obtained from more than 400 combinations of different parameters including ultrasound frequency (20–1000 kHz), acoustic amplitude (0.1–0.3 MPa), static pressure (0.03–0.3 MPa), liquid temperature (283–333 K) and initial bubble radii R_0 (Table 2). An optimum bubble temperature for the production of ·OH radicals is clearly observed at about 5200 ± 200 K.

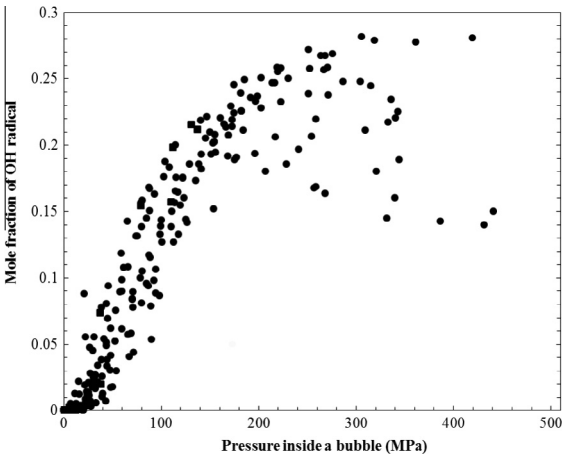

Fig. 5. The correlation between the pressure inside a bubble at the collapse and the mole fraction of ·OH radical formed inside a bubble per collapse for oxygen/water vapor bubbles. The numerical results were obtained from more than 400 combinations of different parameters including ultrasound frequency (20–1000 kHz), acoustic amplitude (0.1–0.3 MPa), static pressure (0.03–0.3 MPa), liquid temperature (283–333 K) and initial bubble radii R_0 (Table 2). An optimum internal pressure is clearly observed at about 250 ± 20 MPa.

and there is no direct correlation between the temperature and pressure distribution and the ambient bubble radius contrary to Figs. 4 and 5 where strong correlations between the mole fraction of ·OH radical and temperature and pressure inside bubbles are observed. Thus, these results (Fig. 6) clearly show that the observed change in the mole fraction of ·OH radical with variation in the bubble temperature (Fig. 4) and pressure (Fig. 5) is not a direct effect of the distribution of the cavitation temperature and pressure with respect to the ambient bubble radius.

Yasui et al. [41], using a more detailed model, predicted an optimum bubble temperature of about 5500 K for the production of the oxidants in an air bubble because, as reported by the authors, for higher bubble temperatures (>5500 K), the oxidants are strongly consumed inside a bubble by oxidizing nitrogen. In our case (O_2

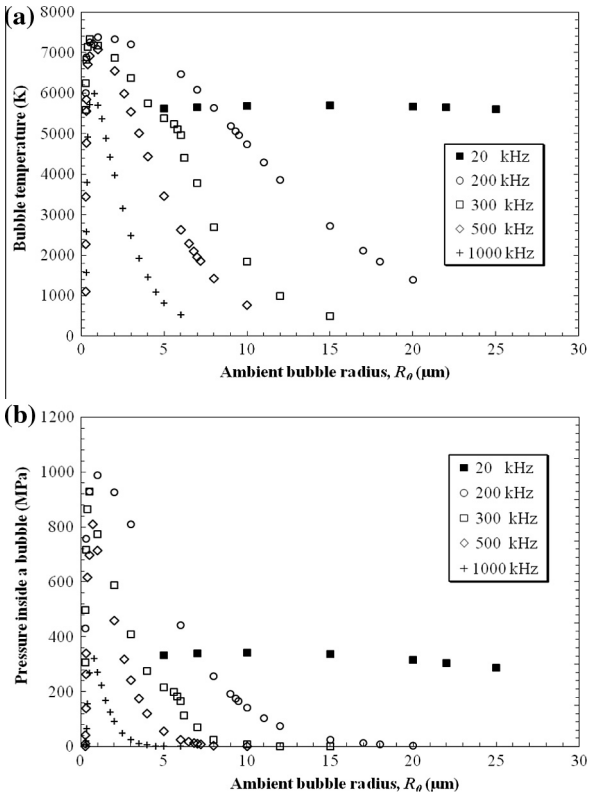

Fig. 6. Distribution of the cavitation bubble temperature (a) and pressure (b) at the collapse for various ambient bubble radii (conditions: frequency: 20–1000 kHz, acoustic aptitude: 0.1 MPa for 20 kHz and 0.3 MPa for the other frequencies, liquid temperature: 293 K, static pressure: 0.1 MPa). It is clearly shown that there is no direct correlation between the temperature and pressure distribution and the ambient bubble radius, which excludes the direct contribution of the bubble temperature and pressure distributions on the trends of Figs. 4 and 5.

bubble), because nitrogen is absent, the existence of an optimum bubble temperature and pressure for the production of ·OH radicals may be attributed to the competition between the reactions of production and those of consumption of ·OH radicals at high temperatures. The determination of the exact reactions for these two processes is difficult because of different operational conditions (combinations between parameters). However, basing on the results of Figs. 4 and 5, it can be seen that for temperatures and pressures less than 4500 K and 180 MPa respectively, linear evolutions of the valleys of points constituting the mole fractions of ·OH radicals created per collapse as function of temperature (Fig. 4) and pressure (Fig. 5) are observed. So, we can make a decision that the reactions of consumption has no significant impacts when the bubble temperature and pressure are less than 4500 K and 180 MPa, respectively and, thus, the reactions of production are always dominated. However, when the bubble temperature and pressure exceed 4500 K and 180 MPa respectively, we observe a decline in the valleys of Figs. 4 and 5, indicating that the reactions of consumption are started to take place by scavenging ·OH radicals. The scavenging effect of the consumption reactions continues to increase with the internal temperature and pressure above 4500 K and 180 MPa to finally yield an optimum temperature of around 5200 K and pressure of around 250 MPa for the production of ·OH radicals. This is possibly the unique reason for the existence of an optimum bubble temperature and pressure for the production of the oxidants, i.e. OH radicals, in the collapsing bubbles.

Finally, we don't optimize the bubble temperature to control it because it is an incontrollable parameter in the cavitation field, but to clarify by numerical simulations, for the first time, for an oxygen bubble that there exists on optimum bubble temperature for the

production of ·OH radicals. This alone constitutes an advance in the field of cavitation used for sonochemistry because the bubble temperature is the paramount parameter that characterizes the cavitation bubbles in acoustical field [15]. Furthermore, the optimum bubble temperature predicted numerically presents in reality the maximum bubble temperature determined experimentally because both, experimental and numerical determinations, are indirect methods based on quantification of the products of sonochemical reaction (i.e. ·OH radical for the numerical determination and ethylene and ethane in the case of methyl radical recombination (MRR) method [15]). Determining the maximum bubble temperature is, thus, critical to understanding the phenomena (sonochemistry, sonoluminescence, etc.) induced by cavitation bubbles in liquids.

4. Conclusion

In this study, we performed a series of simulations of chemical reactions inside an isolated spherical bubble oscillating in water irradiated by an ultrasonic wave. The simulations were performed for diverse combinations (more than 400 points) of various parameters such as ultrasound frequency (20–1000 kHz), acoustic amplitude (up to 0.3 MPa), static pressure (0.03–0.3 MPa) and liquid temperature (283–333 K). The aim of this series of computations is to correlate the production of ·OH radicals to the temperature and pressure inside a collapsing bubble. An optimum bubble temperature of about 5200 ± 200 K and pressure of about 250 ± 20 MPa were found. These predicted values of the bubble temperature and pressure for the production of ·OH radicals are in good agreement with those furnished by the experiments. The competition between the reactions of production and those of consumption of ·OH radicals is the unique reason for the existence of optimum bubble temperature and pressure for the production of the oxidants, i.e. ·OH radicals, inside a collapsing bubbles initially composed of oxygen and water vapor.

Acknowledgements

The financial support by the General Directorate for Scientific Research and Technological Development (PNR project No. 4/D/25) and the Ministry of Higher Education and Scientific Research of Algeria (projects No. J0101120090018 and J0101120120098) is greatly acknowledged.

References

[1] T.J. Mason, J.P. Lorimer, Applied Sonochemistry: The Use of Power Ultrasound in Chemistry and Processing, Wiley-VCH Verlag GmbH, Weinheim, 2002. pp. 25–60.
[2] K.S. Suslick, Y. Didenko, M.M. Fang, T. Hyeon, K.J. Kolbeck, W.B. McNamara, M.M. Mdleleni, M.M. Wong, Acoustic cavitation and its chemical consequences, Phil. Trans. Roy. Soc. A: Math. Phys. Eng. Sci. 357 (1999) 335–353.
[3] K.S. Suslick, Sonochemistry, Kirk-Othmer Encyclopedia of Chemical Technology, John Wiley & Sons, Inc., 2000.
[4] K.S. Suslick, Sonoluminescence and sonochemistry, Encyclopedia of Physical Science and Technology, 3rd ed., R.A. Meyers (ed.), Academic Press, Inc.: San Diego, 2001.
[5] P. Riesz, D. Berdahl, C.L. Christman, Free radical generation by ultrasound in aqueous and nonaqueous solutions, Environ. Health Persp. 64 (1985) 233–252.
[6] M. Ashokkumar, F. Grieser, Single-bubble sonoluminescence – A chemist's overview, Chem. Phys. Chem. 5 (2004) 439–448.
[7] F.R. Young, Sonoluminescence, CRC Press, Boca Raton, Florida, 2005. preface and pp. 45–51.
[8] V. Misík, N. Miyoshi, P. Reisz, EPR-spin trapping of the sonolysis of H_2O/D_2O mixtures: probing the temperatures of cavitation regions, J. Phys. Chem. 99 (1995) 3605–3611.
[9] V. Misík, P. Reisz, EPR study of free radical induced by ultrasound in organic liquids: II. Probing the temperatures of cavitation regions, Ultrason. Sonochem. 3 (1996) 25–37.
[10] K.S. Suslick, D.A. Hammerton, R.E. Cline, The sonochemical hot spot, J. Am. Chem. Soc. 108 (1986) 641–5642.
[11] E.J. Hart, C.H. Fischer, A. Henglein, Sonolysis of hydrocarbons in aqueous solution, Radiat. Phys. Chem. 36 (1990) 511–516.
[12] A. Tauber, G. Mark, H.P. Schuchmann, C. Von Sonntag, Sonolysis of tert-butyl alcohol in aqueous solution, J. Chem. Soc. Perkin Trans. 2 (1999) 1129–1135.
[13] E. Ciawi, J. Rae, M. Ashokkumar, F. Grieser, Determination of temperatures within acoustically generated bubbles in aqueous solutions at different ultrasound frequencies, J. Phys. Chem. B 110 (2006) 13656–13660.
[14] J. Rae, M. Ashokkumar, E. Eulaerts, C. Von Sonntag, J. Reisse, F. Grieser, Estimation of ultrasound induced cavitation bubble temperatures in aqueous solutions, Ultrason. Sonochem. 12 (2005) 325–329.
[15] M. Ashokkumar, The characterization of acoustic cavitation bubbles – An overview, Ultrason. Sonochem. 18 (2011) 864–872.
[16] L.A. Crum, The polytrophic exponent of gas contained within air bubbles pulsating in a liquid, J. Acoust. Soc. Am. 73 (1983) 116–120.
[17] J.B. Keller, I.I. Kolodner, Damping of underwater explosion bubble oscillations, J. Appl. Phys. 27 (1956) 1152–1161.
[18] J.B. Keller, M.J. Miksis, Bubble oscillations of large amplitude, J. Acoust. Soc. Am. 68 (1980) 628–633.
[19] Y.G. Adewuyi, Sonochemistry: environmental science and engineering applications, Ind. Eng. Chem. Res. 40 (2001) 4681–4715.
[20] A.J. Colussi, L.K. Weavers, M.R. Hoffmann, Chemical bubble dynamics and quantitative sonochemistry, J. Phys. Chem. A 102 (1998) 6927–6934.
[21] B.D. Storey, A.J. Szeri, Water vapor, sonoluminescence and sonochemistry, Proc. R. Soc. Lond. A 456 (2000) 1685–1709.
[22] K. Yasui, T. Tuziuti, M. Sivakumar, Y. Iida, Theoretical study of single-bubble sonochemistry, J. Chem. Phys. 122 (2005) 224706.
[23] V. Kamath, A. Prosperetti, F.N. Egolfopoulos, A theoretical study of sonoluminescence, J. Acoust. Soc. Am. 94 (1993) 248–260.
[24] S. Fujikawa, T. Akamatsu, Effects of the non-equilibrium condensation of vapour on the pressure wave produced by the collapse of a bubble in a liquid, J. Fluid Mech. 97 (1980) 481–512.
[25] S. Merouani, O. Hamdaoui, Y. Rezgui, M. Guemini, Computer simulation of chemical reactions occurring in collapsing acoustical bubble dependence of free radicals production on operational conditions, Res. Chem. Intermed. (2013). in press, DOI 10.1007/s11164-013-1240-y.
[26] M.O. Conaire, H.J. Curran, J.M. Simmie, W.J. Pitz, C.K. Westbrook, A comprehensive modeling study of hydrogen oxidation, Int. J. Chem. Kinet. 36 (2004) 603–622.
[27] M.A. Mueller, T.J. Kim, R.A. Yetter, F.L. Dryer, Flow reactor studies and kinetic modeling of the H_2/O_2 reaction, Int. J. Chem. Kinet. 31 (1999) 113–125.
[28] NIST Chemical Kinetics Database, <http://kinetics.nist.gov/index.php> (date last viewed 27/9/2012).
[29] G. Hauke, D. Fuster, C. Dopazo, Dynamic of a single cavitating and reacting bubble, Phys. Rev. E 75 (2007) 066310-1–066310-14.
[30] A. Brotchie, F. Grieser, M. Ashokkumar, Effect of power and frequency on bubble-size distributions in acoustic cavitation, Phys. Rev. Lett. 102 (2009) 084302-1–084302-4.
[31] F. Burdin, N.A. Tsochatzidis, P. Guiraud, A.M. Wilhelm, H. Delmas, Characterisation of the acoustic cavitation cloud by two laser techniques, Ultrason. Sonochem. 6 (1999) 43–51.
[32] N.A. Tsochatzidis, P. Guiraud, A. Wilhelm, H. Delmas, Determination of velocity, size and concentration of ultrasonic cavitation bubbles by the phase-Doppler technique, Chem. Eng. Sci. 56 (2001) 1831–1840.
[33] A. Thiemann, T. Nowak, R. Mettin, F. Holsteyns, A. Lippert, Characterization of an acoustic cavitation bubble structure at 230 kHz, Ultrason. Sonochem. 18 (2011) 595–600.
[34] S. Labouret, J. Frohly, Distribution en tailles des bulles d'un champ de cavitation ultrasonore, 10ème Congrès Français d'Acoustique, Lyon, 2010.
[35] S. Merouani, O. Hamdaoui, Y. Rezgui, M. Guemini, Effects of ultrasound frequency and acoustic amplitude on the size of sonochemically active bubbles –Theoretical study, Ultrason. Sonochem. 20 (2013) 815–819.
[36] K. Yasui, T. Tuziuti, J. Lee, T. Kozuka, A. Towada, The range of ambient radius for an active bubble in sonoluminescence and sonochemical reactions, J. Chem. Phys. 128 (2008) 184705-1–184705-12.
[37] K. Yasui, Influence of ultrasonic frequency on multibubble sonoluminescence, J. Acoust. Soc. Am. 112 (2002) 1405–1413.
[38] W.B. McNamara, Y.T. Didenko, K.S. Suslick, Sonoluminescence temperatures during multi-bubble cavitation, Nature 104 (1999) 772–775.
[39] K.S. Suslick, D.J. Flannigan, Inside a collapsing bubble: sonoluminescence and the conditions during cavitation, Annu. Rev. Phys. Chem. 59 (2008) 659–683.
[40] D.J. Flannigan, S.D. Hopkins, C.G. Camara, S.J. Putterman, K.S. Suslick, Measurement of pressure and density inside a single sonoluminescing bubble, Phys. Rev. Lett. 96 (2006) 204301-1–204301-4.
[41] K. Yasui, T. Tuziuti, Y. Iida, Optimum bubble temperature for the sonochimical production of oxidants, Ultrasonics 42 (2004) 579–584.